most of the core methane will remain within the satellite after differentiation, irrespective of the thickness (or existence[19]) of the ocean. First, we show that the material originally accreted into the primordial core as SIMH will be a mixture of ice and MH-III under the P–T conditions at the end of accretion. As we have also established that the SIMH to MH-II and MH-II to MH-III transitions are both readily reversible, gravitational differentiation after core overturn will return all the core methane to SIMH as the methane-containing component rises above the final core and passes through the layer of ice phases at the bottom of the mantle (which are denser, as Fig. 2 shows). The outcome will be a layer of SIMH some 100 km thick either just below or just above the ammonia–water ocean—the ocean's density is not well enough known to determine which. In either case, this large amount of SIMH will be stable to the base of the surface ice layer (where the pressure is estimated to be 0.1 GPa (ref. 2)).

These results imply that it is unlikely that Titan has surface pools of methane. Instead, the SIMH layer provides a possible long-term source of atmospheric methane through convective processes such as cryovulcanism[1,2,20]. The presence of an approximately 100 km thick SIMH layer will also have an impact on the modelling of thermal and rheological processes[2]. Furthermore, the incorporation into the SIMH layer of a substantial amount of water that was previously believed to be free will increase the ammonia content of the ammonia–water ocean and hence increase its thickness. □

Received 27 June 2000; accepted 26 January 2001.

1. Lunine, J. I. & Stevenson, D. J. Clathrate and ammonia hydrates at high-pressure—application to the origin of methane on Titan. *Icarus* **70,** 61–77 (1987).
2. Grasset, O., Sotin, C. & Deschamps, F. On the internal structure and dynamics of Titan. *Planet. Space Sci.* **48,** 617–636 (2000).
3. Lunine, J. I. & Stevenson, D J. Thermodynamics of clathrate hydrate at low and high pressures with application to the outer solar system. *Astrophys. J. Suppl. Ser.* **58,** 493–531 (1985).
4. Hirai, H. *et al.* Methane hydrate behaviour under high pressure. *J. Phys. Chem. B* **104,** 1429–1433 (2000).
5. Hirai, H. *et al.* Methane hydrate, amoeba or a sponge made of water molecules. *Chem. Phys. Lett.* **325,** 490–498 (2000).
6. Lorenz, R. D. The weather on Titan. *Science* **290,** 467–468 (2000).
7. Lunine, J. I. Does Titan have an ocean? A review of current understanding of Titan's surface. *Rev. Geophys.* **31,** 133–149 (1993).
8. Gutt, C. *et al.* The structure of deuterated methane hydrate. *J. Chem. Phys.* **113,** 4713–4721 (2000).
9. van der Waals, J. H. Statistical mechanics of clathrate compounds.*Trans. Faraday Soc.* **52,** 184 (1956).
10. van der Waals, J. H. & Platteeuw, J. C. Clathrate solutions. *Adv. Chem. Phys.* **2,** 1 (1959).
11. Dyadin, Y. A., Aladko, E. Y. & Larionov, E. G. Decomposition of methane hydrates up to 15 kbar. *Mendeleev Commun.* **7,** 34–35 (1997).
12. Pistorius, C. W., Pistorius, M. C., Blakey, J. P. & Adimiraal, L. J. Melting curve of ice VII to 200 kbar. *J. Chem. Phys.* **38,** 600 (1963).
13. Udachin, K. A., Ratcliffe, C. I., Enright, G. D. & Ripmeester, J. A. Structure H Hydrate: a single crystal diffraction study of 2,2 dimethylpentane.5(Xe,H_2S).34H_2O. *Supramol. Chem.* **8,** 173–176 (1997).
14. Chou, I. M. *et al.* Transformations in methane hydrates. *Proc. Natl Acad. Sci.* **97,** 13484–13487 (2000).
15. Dyadin, Y. A. *et al.* Clathrate hydrates of hydrogen and neon. *Mendeleev Commun.* **5,** 209–210 (1999).
16. Dyadin, Y. A., Larionov, E. G., Mirinski, D. S., Mikina, T. V. & Starostina, L. I. Clathrate formation in the Ar-H_2O system under pressures up to 15,000 bar. *Mendeleev Commun.* **7,** 32–34 (1997).
17. Lotz, H. T. & Schouten, J. A. Clathrate hydrates in the system H_2O-Ar at pressures and temperatures up to 30 kbar and 140 °C. *J. Chem. Phys.* **111,** 10242–10247 (1999).
18. van Hinsberg, M. G. E., Scheerboom, M. I. M. & Schouten, J. A. The vibrational spectra of N_2 in clathrate-hydrates: A new high-pressure phase transition. *J. Chem. Phys.* **99,** 752–754 (1993).
19. Grasset, O. & Sotin, C. The cooling rate of a liquid shell in Titan's interior. *Icarus* **123,** 101–112 (1996).
20. Stevenson, D. J. in *Proceedings of Symposium on Titan* 29–33 (European Space Agency Special Publication SP-338, Toulouse, 1992).
21. Handa, Y. P. Compositions, enthalpies of dissociation, and heat-capacities in the range 85K–270K for clathrate hydrates of methane, ethane, and propane, and enthalpy of dissociation of isobutane hydrate, as determined by a heat-flow calorimeter. *J. Chem. Therm.* **18,** 915–921 (1986).
22. Nelmes, R. J. *et al.* Structure studies at high pressure using neutron powder diffraction. *Trans. Am. Cryst. Ass.* **29,** 19–27 (1993).
23. *PEARL—Pressure and Engineering Research Line* 28–29 ISIS'97 Rutherford Appleton Laboratory Report RAL-TR-97-050 (RAL, Didcot, 1997).
24. Nelmes, R. J. & McMahon, M. I. High-pressure powder diffraction on synchrotron sources. *J. Synch. Rad.* **1,** 69–73 (1994).

Acknowledgements

We thank D. J. Francis, T. Bovornratanaraks and M. Hanfland for assistance with experiments, and O. Grasset and D. J. Stevenson for helpful discussions of their work. Our work is funded by a research grant from the EPSRC, and supported by CCLRC through access to beamtime and other resources.

Correspondence and requests for materials should be addressed to J. S. L.. (e-mail: J.Loveday@ed.ac.uk).

A thermodynamic connection to the fragility of glass-forming liquids

L.-M. Martinez & C. A. Angell

Department of Chemistry and Biochemistry, Arizona State University, Tempe, Arizona 85287-1604, USA

Although liquids normally crystallize on cooling, there are members of all liquid types (including molecular, ionic and metallic) that supercool and then solidify at their glass transition temperature, T_g. This continuous solidification process exhibits great diversity within each class of liquid—both in the steepness of the viscosity–temperature profile, and in the rate at which the excess entropy of the liquid over the crystalline phase changes as T_g is approached. However, the source of the diversity is unknown. The viscosity and associated relaxation time behaviour have been classified between 'strong' and 'fragile' extremes, using T_g as a scaling parameter[1], but attempts to correlate such kinetic properties with the thermodynamic behaviour have been controversial[2,3]. Here we show that the kinetic fragility can be correlated with a scaled quantity representing excess entropy, using data over the entire fragility range and embracing liquids of all classes. The excess entropy used in our correlation contains both configurational and vibration-related contributions. In order to reconcile our correlation with existing theory and simulations, we propose that variations in the fragility of liquids originate in differences between their vibrational heat capacities, harmonic and anharmonic, which we interpret in terms of an energy landscape. The differences evidently relate to behaviour of low-energy modes near and below the boson peak.

The understanding of fluidity and diffusion in viscous liquids is in a state of flux. Formerly considered as a problem in energy-barrier crossing—and hence strictly kinetic in nature—it is now being suggested by molecular-dynamics (MD) studies that liquid diffusion is a process dominated by thermodynamic factors. Nearly three years ago, Sastry *et al.*[4] presented an 'inherent structures' analysis of MD data on a binary Lennard–Jones liquid (BMLJ), showing that two key dynamic features could be related to the static structure through the potential-energy hypersurface features that the liquid explores with highest probability at different temperatures. These were the onset of 'super-Arrhenius' behaviour, and the location of the mode-coupling theory critical temperature T_c (obtained by power-law fitting of the diffusivity versus temperature relation). An implication that the landscape excitation profile would provide a measure of liquid fragility that was basically thermodynamic was quantified by Speedy, who derived[5] an expression for thermodynamic fragility in which the excess entropy 'frozen in' at the kinetic glass transition plays an important scaling role.

This implication was also followed up by Ito *et al.*[2], who recast Kauzmann's normalized entropy data in a T_g-scaled form that has the same appearance as the common kinetic fragility plot. Their plot also assigns a key scaling role to the excess entropy frozen in at T_g. They observed, qualitatively, that the ordering of liquids was the same in both kinetic and thermodynamic manifestations. This notion was however immediately contested by Ngai *et al.*[3,6]. These authors suggested, from an analysis of the dielectric relaxation times and entropies of nine molecular liquids[3], that the correlation was unreliable at best and, in the case of polymeric liquids[6], was not applicable. Here we provide data on a much wider set, which includes all the cases of ref. 3, in order to clarify this problem. Clarification is demanded because, if kinetic fragility is indeed dominated by thermodynamics in the 'normal' case, then a significant simplification of the whole fragility phenomenon

(and also the topography of the potential-energy surface) is at hand.

We start with a proviso about thermodynamic fragility. In the definition of this quantity in ref. 2, one advantage of the kinetic fragility is missing. This is the manner in which the kinetic fragility is made independent of the properties of the crystal phase. By using T_g as a reference temperature instead of the melting point, the kinetic fragility is made an entirely liquid-state quantity. In the thermodynamic fragility analogue defined by Ito *et al.*[2], this reference temperature scaling advantage is maintained. Unfortunately, however, in our attempt to select the important part of the entropy for liquid-state behaviour (that is, S_{ex}, the part in excess of the entropy of the fixed structure, which is usually taken as that of the crystal), we find ourselves still at the mercy of idiosyncrasies of the crystal phase. This is because changes of vibrational entropy on fusion will affect the entropy of fusion, to which S_{ex} is always referred (except in MD evaluations[7–13]).

The outstanding case is that of SiO_2 and certain silicates[14,15] (Fig. 2 legend). A similar problem with chain polymer crystals, in which the force-constant distribution must be even more heterogeneous than in silicate crystals, is perhaps the reason that attempts to correlate Vogel–Fulcher and Kauzmann temperatures, respectively T_o and T_K, (see Methods) have never met with much success for polymers. It might also explain why, for polymers, Roland *et al.*[6] found such disarray in the correlation we are discussing here. Until we can obtain the entropy of the glass at T_g using the ideal-gas reference state, as in MD studies[7–13], we must expect to find some serious anomalies. We do not think this should prevent us from making an attempt to see the broader picture. We hope that the conclusions about the source of fragility that we report here will justify our tolerance of some cases which, without the proviso just made, might seem to sustain the conclusions of refs 3 and 6. Why not avoid the crystal problem by reverting to the use of the constant-pressure heat capacity ratio $C_{p,\mathrm{liquid}}/C_{p,\mathrm{glass}}$, a purely liquid-state property, as in the past[1]? Speedy's argument[5], and the Adam–Gibbs equation[16] (the form of which has now been strongly supported by MD simulations[11–13]), show that the scaled entropy quantity is required.

With the foregoing proviso in mind, we will now show that comparison of viscosity data with thermodynamic data on the same liquids broadly confirms the original suggestion[2]. As shown in the

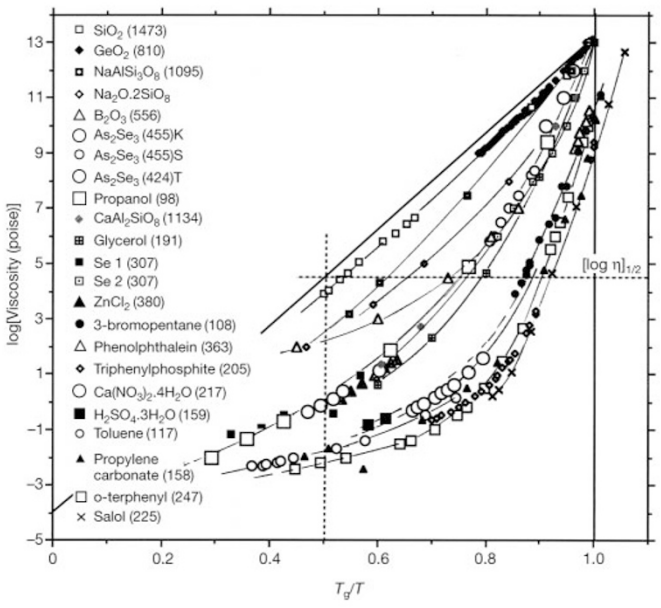

Figure 1 T_g-scaled Arrhenius plot for liquids of every class for which thermodynamic data are also available. The scaling parameter used here and in Fig. 2 is the normal calorimetric T_g at which the enthalpy relaxation time is ~200 s (values are shown in parentheses in the key to the figure). The horizontal line is drawn half way between 10^{13} poise (characteristic of the glass transition for non-fragile liquids), and 10^{-4} poise (which is the roughly common high-temperature limiting value). The log($\eta_{1/2}$) line is used to obtain the $F_{1/2}$ fragility (kinetic) by the definition $F_{1/2} = 2T_g/T_{1/2} - 1$. This is recommended[18] as the most reliable metric of the deviation from Arrhenius behaviour, which is central to the fragility concept. We note that the kinetic fragilities of liquids whose viscosities are less than 10^{12} Pa s at their calorimetric T_g (due to small shear moduli or viscosity/structure decoupling) are exaggerated by this construction. Fragility plots using relaxation times instead of viscosities are simpler because they all pass through the same point at the reference temperature[3,18]. Relaxation time data, however, are much less generally available than viscosity data, and dielectric relaxation times are not available for ionic or covalent liquids. We have also (L.-M.M. *et al.*, unpublished work) made a modified version of this plot where we take into account the mechanical relaxation times that are available for a smaller set of liquids. (Relaxation times under shear are proportional to viscosities via a Maxwell relation in which the proportionality constant (G_∞, the high-frequency shear modulus) has only a weak temperature dependence). The available mechanical relaxation time data will be presented elsewhere.

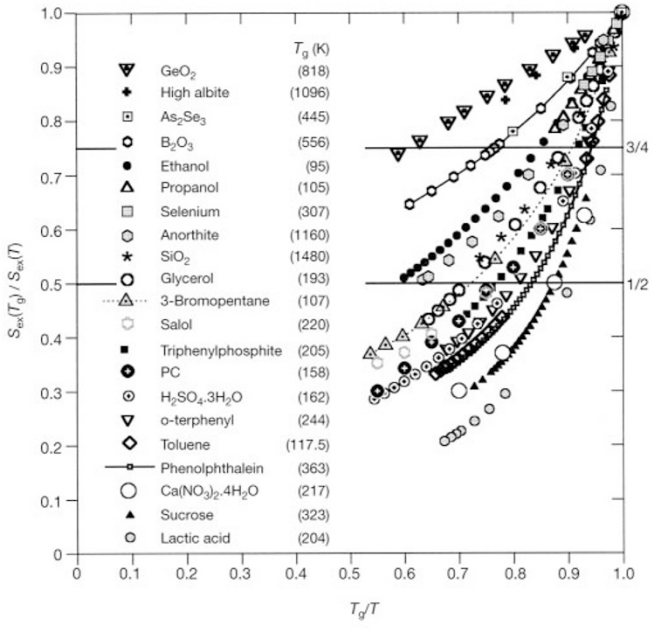

Figure 2 Plots of scaled excess entropy versus T_g-scaled inverse temperature. Data are shown for members of every class of glass-forming systems except metals (for which appropriate compound entropy data are unavailable). The excess of liquid entropy over that of the crystal, S_{ex}, at different temperatures T_g/T above T_g is shown scaled by the excess entropy at T_g, $S_{ex}(T_g)$, so that the figure appears similar to Fig. 1. The lines drawn at the 0.5 and 0.75 marks are used to obtain thermodynamic fragilities $F_{1/2}$ and $F_{3/4}$ for comparison with the kinetic quantities. The latter is preferable, as it does not require any data extrapolations (for strong liquids) for its determination. We note the anomalous position of SiO_2, which is the strongest liquid in Fig. 1. This anomaly has been pointed out before, by Richet[14,15], in his consideration of the thermodynamics of geosilicate glass-formers. The anomaly arises because in silica, almost uniquely[14], the vibrational entropy of the glass is much less than those of the crystalline polymorphs. This has the consequence that the entropy of fusion, and therefore the computed excess entropy of the glass at T_g (which scales the liquid entropy), is confusingly small. The problem would not arise if the glass entropy could be assessed by either of the all-liquid routes used in MD computer-simulation studies[7–13]. Richet noted that it is not possible to find a systematic relation between the entropy of fusion and the liquid properties in geochemical melts because of such complexities in the crystal thermodynamics. Comparable anomalies, having different origins, attend some other complex silicates. However, Richet showed that, if attention is focused on the increase in heat capacity at T_g (which, like the viscosity, is a purely liquid state property), then kinetic fragility and thermodynamic fragility, judged by $C_{p,\mathrm{liquid}}/C_{p,\mathrm{glass}}$ at T_g, are systematically related for these mineral liquids—which are mostly 'strong' in character.

Methods section, this is consistent with the earlier finding[17] that the thermodynamic and kinetic ground-state temperatures are mostly equal.

Figures 1 and 2 show plots of the kinetic fragility and thermodynamic fragility of the liquids that are listed in the legends (in order of increasing fragility). We note that the order of the curves in Figs 1 and 2 is the same with few exceptions, though the exceptions may be striking—for example, SiO_2 in Fig. 2 (see legend).

To make a more quantitative comparison, we may use the intersections of the individual data sets with the mid-range line indicated on each figure. This gives us the $F_{1/2}$ fragility, the advantages and measurement of which have been discussed elsewhere[18] for the simpler case of relaxation times. For the thermodynamic fragility it is preferable to use the 3/4 line, as this avoids the need for extrapolations in the case of strong liquids.

The thermodynamic and kinetic fragilities, defined in this way, are compared in Fig. 3. While the exceptions are of course still present, most of the substances analysed show thermodynamic fragilities that are well correlated with their kinetic fragilities. The exceptions identified in ref. 3 weigh less heavily among the larger number of simply related cases. We note the wide variety of different liquid types of intermediate fragility that cluster around selenium in Fig. 3.

Figure 3 shows a much closer correlation than we would have expected from the application of the Adam–Gibbs equation[16], which contains a specifically kinetic parameter (see below). We previously argued[1] that this parameter would exert an independent

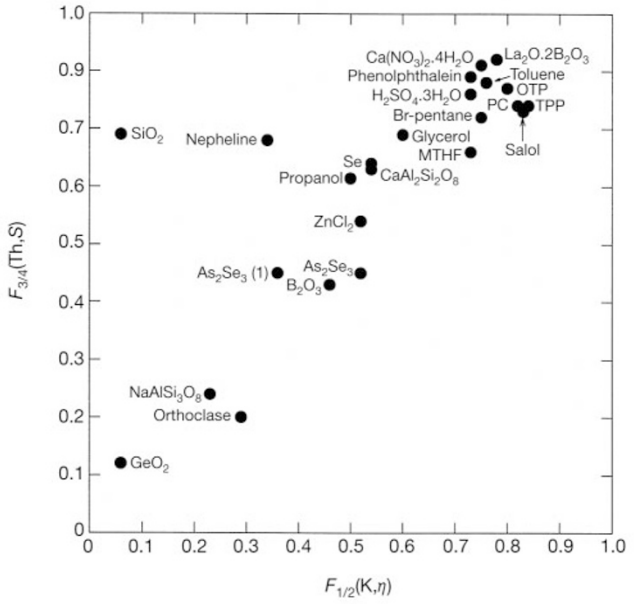

Figure 3 Correlation of the thermodynamic and kinetic $F_{1/2}$ fragilities from Figs 1 and 2. Sucrose and lactic acid are excepted for lack of reliable viscosity data. The thermodynamic fragilities of strong liquids, for example, SiO_2, are very susceptible to distortion due to vibrational entropy differences of crystal and glass, and would be better assessed using heat capacity jumps at the glass temperature (see Fig. 2 legend). This figure contains additional data ($ZnCl_2$, $La_2O{\cdot}2B_2O_3$, MTHF) not included in Figs 1 and 2 for reason of crowding. The present figure contains all of the examples included in ref. 2, which are here concentrated in the top right-hand corner (glycerol and above). We have added inorganic liquids, for example, $Ca(NO_3)_2{\cdot}4H_2O$, $H_2SO_4{\cdot}3H_2O$, $La_2O{\cdot}2B_2O_3$, to this area. In ref. 3, Fig. 3 insert, MTHF is the outstanding exception, 3-bromopentane was misplotted, and only one of the two toluene points has the appropriate excess entropy. In ref. 17, propanol, salol and phenolphthalein were exceptions. On the scale of the present figure these deviations are less prominent. MTHF, methyl tetrahydrofuran; TPP, triphenyl phosphite; OTP, orthoterphenyl. (Th, S) indicates a thermodynamic assessment based on entropy data, and (K, η) indicates a kinetic assessment based on viscosity data.

control of the fragility but it now seems that the effect is minor. However, before anything can be made of this simplification in both phenomenology and implied configuration-space topography[19,20], we must face the fact that our correlation is not the one that even a simplified Adam–Gibbs equation would predict. This is because the excess entropy that we have used to construct Fig. 2 is not the quantity that should appear in the Adam–Gibbs equation, even though it is the quantity that has been used in most of its experimental tests. We now analyse the implications of this difference.

The Adam–Gibbs equation for the relaxation time τ of a dense liquid[16], which has been tested and found to be of valid form in three recent computer simulation studies[7,11–13], is

$$\tau(\sim TD^{-1}) = \tau_o \exp(C/TS_c) \quad (1)$$

where D is the diffusivity (and the T multiplier takes into account the Einstein relation between diffusivity and mobility), τ_0 is a constant of order 10^{-14} s, C is a constant which contains an energy barrier per particle, and S_c is the configurational entropy. S_c is that part of the entropy of a pure liquid which is determined by the plethora of possible distinct packing states accessible at the temperature T. It is related logarithmically to the number of minima on the Goldstein–Stillinger potential-energy hypersurface of the system's configuration space[19,20]. It is accessible by computer simulation studies when correctly performed[7–13]. While it has often been assumed that S_c can be approximated by the difference in entropy between liquid and crystal, it has been known since Goldstein's analysis[21] of entropy change in glasses between T_g and 0 K that this is a rather poor approximation in many cases. According to such studies[21,22], the configurational component of the excess entropy may be as small as 40% of the excess entropy at T_g, with no pattern obvious for different types of liquids. Sastry's simulations[13] help to explain why. A reason for ignoring these observations has no doubt been the fact that the Adam–Gibbs equation usually tests well (that is, linearizes the relaxation time or diffusivity data near T_g) using the easily accessible excess entropy[23–25,17,18]. Figure 3 provides another example of this success. Yet MD simulation studies of both SPC-E water[11] and BMLJ liquid[12,13] find that equation (1) holds as written. In neither case is the excess entropy equal to the configurational entropy. How is it that the Adam–Gibbs equation can be satisfied for both quantities?

The answer to this question must be that, as the temperature rises above T_g, S_c and S_{ex} change with temperature proportionally (for example, $S_{ex} = aS_c(T - T_K)$ where T_K is the Kauzmann vanishing S_{ex} temperature. When the rate of change is high, the liquid is fragile (Fig. 2). From these two statements we can deduce much about heat capacity and the origin of fragility. An increase in vibrational (or anharmonicity) entropy in excess of the crystal, as the structure changes above T_g, must promote a corresponding increase in configurational entropy (hence a decrease in τ), at least in the range over which the experimental tests of equation (1)[17,18,23–26] have been made (that is, between T_g and the melting point at about $\sim 1.5T_g$) (L.M.-M. *et al.*, unpublished results). Here we present the argument graphically, in Fig. 4, using the configuration-space energy landscape concepts as developed in refs 4, 19, 20 and 27. We have recently learned that both S. Sastry (personal communication) and Starr *et al.*[31] have demonstrated in simulations the proportionality between S_c and S_{ex} that we have proposed here.

The generation of extra vibrational entropy in the liquid—due to the change in shape of the inherent structure basins (Fig. 4a) that the system 'visits' at higher temperatures—provides an additional drive towards the higher-energy states over that provided by the multiplicity of basins alone. This is dictated by the Gibbs free-energy function $G = H - TS$, where H is enthalpy and S is entropy, which must be minimized at each temperature for the liquid to be in equilibrium. We note that, because we are discussing the results of Figs 1–3, we are depicting the energy profile for a constant-pressure system, which therefore has one extra dimension—volume—relative

to the usual isochoric landscape (hence we refer to Gibbs, rather than Helmholtz, free energy). The more rapidly the landscape is ascended, the more rapidly the configurational entropy is excited. According to equation (1) this would imply more fragile liquid behaviour, but in fact this depends on the scaling principle used in the comparison and on which of S_c or S_{ex} is the most important. The change in basin shape with basin energy is a key ingredient in determining water thermodynamics[28] and diffusivity temperature dependence[11], and BMLJ aging kinetics[31]. We expect it also to be, along with the other factors $k_B \ln W$ (where W is the "number of glasses"[5] and k_B the Boltzmann constant) and the width of the basin energy distribution identified by Sastry[13], a key ingredient in determining the liquid fragility.

For studies conducted at constant volume, as is customary in computer simulations[4,8–13,28,31], a very different scenario is revealed by Sastry's recent study of BMLJ[13]. There the excess vibrational entropy temperature dependence can play an opposing role. This difference needs to be borne in mind when comparing results of simulations and experiments. It implies for fragile liquids the relation $C_{p,ex} > C_{c,p} > C_{c,v} > C_{v,ex}$ (where C_c is the configurational heat capacity).

Figure 4b shows how extrapolations of either total excess entropy, or the configurational component of the excess entropy, should yield the same Kauzmann temperature. It also shows why equation (1) should linearize the data, irrespective of whether excess entropy or configurational entropy is used, and also why—in correlations of thermodynamic fragility with the kinetic quantity—excess entropy should serve as well as configurational entropy. Experimental verification of the qualitative features of Fig. 4b is available in the neutron-scattering study of selenium by Phillips *et al.*[29] (see their Fig. 4). The origin of the excess vibrational entropy is there seen to lie in changes of the density of states (DOS) in the vicinity of the boson peak, as may also be deduced from refs 21 and 22. In SiO_2 (the strong extreme), the opposite changes in the DOS above T_g are found[30]. □

Methods

We support our claim that kinetic, and entropy-based thermodynamic, fragilities are closely related, using three different approaches as detailed below. These involve both experimental and MD computer-simulation data sources. Only the third, experiment-based, approach is detailed here.

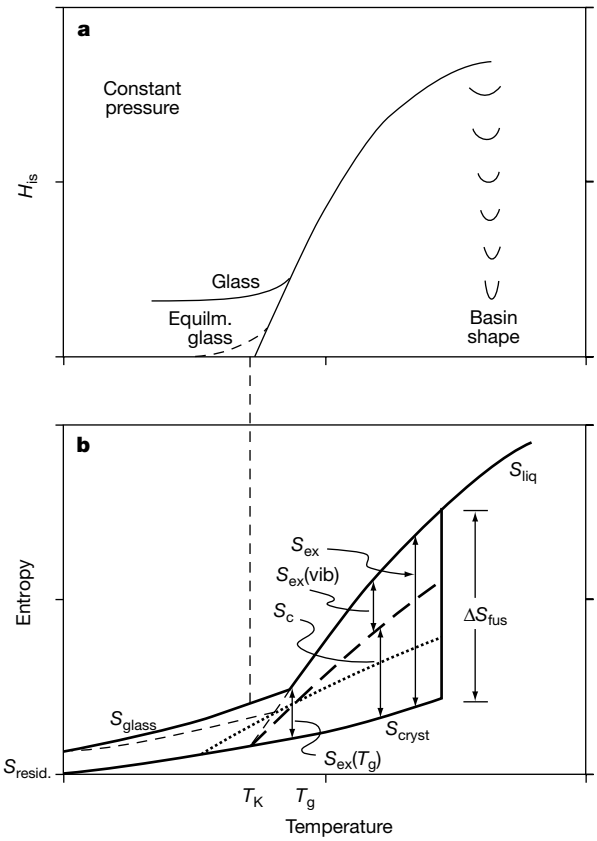

Figure 4 Graphical explanation of how high liquid fragility originates in the change of energy landscape 'basin shape' (hence of the vibrational density of states) during thermal excitation to high potential energies. **a**, Depiction of the inherent structure enthalpy H_s profile for a one-component system during heating from 0 K to above the melting point at constant pressure. Changes in shape of the basins visited with greatest probability[4] at each temperature and volume are depicted to the right of the excitation profile. These become progressively shallower (density of states slanted to lower frequencies) as temperature increases and the system expands. **b**, Entropy versus temperature for the system depicted in **a**, contrasting the monotonic increase of the system entropy, S_{cryst}, when in the crystal basin, with the behaviour of amorphous phases, both strong and fragile. The glass is depicted as having excess entropy S_{resid} at 0 K but a larger S_{ex} at T_g. This is due to the vibrational density of states of the glass being richer in low-frequency modes than that of the crystal. Above T_g the vibrational excess entropy S_{ex} (vib) increases more rapidly than below T_g due to the system having access to basins of different shape as depicted in **a**. This access to additional vibrational entropy provides an additional TS drive which must be balanced by more rapid increase in enthalpy H, than in the case where all basins have the same shape (dotted line). The division of the excess entropy into its configurational and vibrational components is made by the heavy dashed line. In the case of constant basin shape (strong liquid), the drive to higher enthalpies comes only from the configurational entropy, that is, TS_c. The change in S_{ex}, which is also S_c in this case, is depicted as a dotted line. We note that, for variable basin shape, the increased rate of excitation of vibrational entropy has increased the rate of generation of configurational entropy, as well as that of the excess entropy. T_g/T_K must therefore be smaller for this case, hence the fragility larger. Compare with Fig. 4 of ref. 29. The increase in entropy at the melting point ΔS_{fus}, to give the liquid entropy S_{liq}, is seen to contain both configurational and vibration-related components in the case of fragile liquids.

(1) The correlation of kinetic and entropy-based thermodynamic fragilities is implied by the repeated analyses of the calorimetric and kinetic behaviour of liquids (not polymers) of different classes that extract 'ground state temperatures' from the data and find them to have very similar values. We refer to T_K (where the supercooling liquid entropy extrapolates to the crystal entropy) and T_o (where the viscosity extrapolates to infinity by the Vogel–Fulcher–Tammann equation). Ref. 17 describes some 30 cases where $T_o = T_K$ within ± 3% despite several pronounced exceptions). As the ratio T_g / T_o is often taken as a measure of fragility[17], it is clear that $T_K \approx T_o$ implies that kinetic fragility and thermodynamic fragility T_g/T_K are the same, with some pronounced exceptions. This means that either the physically constrained analysis leading to $T_o \approx T_K$ is flawed, or that the analysis of Ngai[3] and co-workers, being limited to dielectric relaxation of molecular liquids, and containing some misplots (see Fig. 3 legend), has distorted the overall picture.

(2) $T_o \approx T_K$ is also a recent result of MD computer-simulation studies on well defined systems[11–13]. Although the number of systems studied is small, the results are important because the identity of T_o and T_K is obtained using all-amorphous phase calculations; that is, there is no reliance on fusion entropy data.

(3) Both of the above arguments are weakened by the fact that they depend on extrapolations beyond the range of experimental or simulation data. To avoid this, and at the same time to obtain a more complete picture than given in refs 2 and 3, we compare wide-ranging data on some 25 liquids from the fields of geochemistry (liquid silicates), covalent semiconductors (liquid chalcogenides), molecular liquids, and molten ionic hydrates, salts and oxides, and including all the systems analysed by Ngai and Yamamuro[3]. Unlike the cases in ref. 3, the present data set covers the whole known fragility range. The quantities studied are the shear viscosities and the excess of the liquid entropy over the crystal entropy measured at the same temperature, and uncorrected in any manner. We note that S_{ex} in ref. 22 is not the same quantity as in the present work. It requires quantitative knowledge of the residual entropy at 0 K for its assessment. Also, in ref. 26 an attempt was made to separate out vibrational contributions to the entropy of the liquid above T_g in order to obtain S_c (for use in the Adam–Gibbs equation (equation (1)) by using a function fitted to the heat capacity of the glass. This yields a quantity which is neither S_c nor S_{ex} because the procedure does not consider the introduction of new low frequencies above T_g, which is central to our conclusions.

The quality of data used in this study is variable, ranging from very high, in the case of adiabatic calorimetry data on molecular liquids (data cited in ref. 3) and some high temperature substances (B_2O_3), to moderate, in the case of high-temperature differential scanning calorimeter (DSC) and drop calorimetry data on minerals. Reference sources are available from the authors. Both data sets are presented (Figs 1 and 2) as functions of inverse temperature scaled by the calorimetric onset T_g for the substance, as measured during upscan at 10 K min^{-1} (after previous continuous cooling at the same rate). This corresponds to scaling by the temperature at which the enthalpy relaxation time is approximately 200 s (refs 17, 18).

Received 10 November 2000; accepted 29 January 2001.

1. Angell, C. A. Relaxation in liquids, polymers and plastic crystals - strong/fragile patterns and problems. *J. Non-Cryst. Solids* **131-133,** 13–31 (1991).
2. Ito, K., Moynihan, C. T. & Angell, C. A. Thermodynamic determination of fragility in liquids and a fragile-to-strong liquid transition in water. *Nature* **398,** 492–495 (1999).
3. Ngai, K. L. & Yamamuro, O. Thermodynamic fragility and kinetic fragility in supercooled liquids: a missing link. *J. Chem. Phys.* **111,** 10403–10406 (1999).
4. Sastry, S., Debenedetti, P. G. & Stillinger, F. H. Signatures of distinct dynamical regimes in the energy landscape of a glassforming liquid. *Nature* **393,** 554–557 (1998).
5. Speedy, R. J. Relations between a liquid and its glasses. *J. Phys. Chem. B* **103,** 4060–4065 (1999).
6. Roland, C. M., Santangelo, P. G. & Ngai, K. L. The application of the energy landscape model to polymers. *J. Chem. Phys.* **111,** 5593–5598 (1999).
7. Speedy, R. J. The hard sphere glass transition. *Mol. Phys.* **95,** 169–178 (1998).
8. Sciortino, F., Kob, W. & Tartaglia, P. Inherent structure entropy of supercooled liquids. *Phys. Rev. Lett.* **83,** 3214–3217 (1999).
9. Buechner, S. & Heuer, A. The potential energy landscape of a model glassformer: thermodynamics, anharmonicities, and finite size effects. *Phys. Rev. E* **60,** 6507–6518 (1999).
10. Coluzzi, B., Verrocchio, P., Mezard, M. & Parisi, G. Lennard-Jones binary mixture: a thermodynamical approach to glass transition. *J. Chem. Phys.* **112,** 2933–2944 (2000).
11. Scala, A., Starr, F., La Nave, E., Sciortino, F. & Stanley, H. E. Configurational entropy and diffusion of supercooled water. *Nature* **406,** 166–169 (2000).
12. Sastry, S. Liquid limits: the glass transition and liquid-gas spinodal boundaries of metastable liquids. *Phys. Rev. Lett.* **85,** 590–593 (2000).
13. Sastry, S. The relationship between fragility, configurational entropy and the potential energy landscape of glassforming liquids. *Nature* **409,** 164–167 (2001).
14. Richet, P. Viscosity and configurational entropy of silicate melts. *Geochim. Cosmochim. Acta* **48,** 471–483 (1984).
15. Richet, P. & Bottinga, Y. Glass transitions and thermodynamic properties of amorphous SiO_2, $NaAlSi_nO_{2n+2}$ and $KAlSi_3O_8$. *Geochim. Cosmochim. Acta* **48,** 453–470 (1984).
16. Adam, G. & Gibbs, J. H. On the temperature dependence of cooperative relaxation properties in glassforming liquids. *J. Chem. Phys.* **43,** 139–146 (1965).
17. Angell, C. A. Entropy and fragility in supercooled liquids. *J. Res. NIST* **102,** 171–185 (1997).
18. Richert, R. & Angell, C. A. Dynamics of glassforming liquids. IV: On the link between molecular dynamics and configurational entropy. *J. Chem. Phys.* **108,** 9016–9026 (1998).
19. Goldstein, M. Viscous liquids and the glass transition: a potential energy barrier picture. *J. Chem. Phys.* **51,** 3728–3729 (1969).
20. Stillinger, F. H. & Weber, T. A. Packing structures and transitions in liquids and solids. *Science* **225,** 983–989 (1984).
21. Goldstein, M. Viscous liquids and the glass transition: sources of the excess heat capacity. *J. Chem. Phys.* **64,** 4767–4773 (1976).
22. Johari, G. P. Contributions to the entropy of a glass and liquid, and the dielectric relaxation time. *J. Chem. Phys.* **112,** 7518–7523 (2000).
23. Greet, R. J. & Turnbull, D. Test of Adam-Gibbs liquid viscosity model with *o*-terphenyl specific-heat data. *J. Chem. Phys.* **47,** 2185–2190 (1967).
24. Magill, J. H. Physical properties of aromatic hydrocarbons. III. A test of the Adam-Gibbs relaxation model for glass formers based on the heat-capacity data of 1,3,5-tri-α-naphthylbenzene. *J. Chem. Phys.* **47,** 2802–2807 (1967).
25. Takahara, S., Yamamuro, O. & Suga, H. Heat capacities and glass transitions of 1-propanol and 3-methyl pentane: new evidence for the entropy theory. *J. Non-Cryst. Solids* **171,** 259–270 (1994).
26. Takahara, S., Yamamuro, O. & Matsuo, T. Calorimetric study of 3-bromopentane—correlation between structural relaxation time and configurational entropy. *J. Phys. Chem.* **99,** 9580–9592 (1995).
27. Angell, C. A. Liquid landscapes. *Nature* **393,** 521–522 (1998).
28. Starr, F. W. *et al.* Thermodynamic and structural aspects of the potential energy surface of simulated water. *Phys. Rev. E.* (in the press); also preprint arXiv:cond-mat/0007487 on ⟨xxx.lanl.gov⟩ (2000).
29. Phillips, W. A., Buchenau, U., Nücker, N., Dianou, A. J. & Petry, W. Dynamics of glassy and liquid selenium. *Phys. Rev. Lett.* **63,** 2381–2384 (1989).
30. Wischnewski, A., Buchenau, U., Dianoux, A. J., Kamitakahara, W. A. & Zarestky, J. L. Neutron scattering analysis of low-frequency modes in silica. *Phil. Mag. B* **77,** 579–589 (1998).
31. Kob, W., Sciortino, F. & Tartaglia, P. Aging as dynamics in configuration space. *Europhys. Lett.* **49,** 590–596 (2000).

Acknowledgements

We thank S. Sastry, R. Speedy and F. Sciortino for comments and criticisms. This work was supported by the NSF, Division of Materials Research, Solid State Chemistry program.

Correspondence and requests for materials should be addressed to C.A.A. (e-mail: caa@asu.edu).

Intermittent dislocation flow in viscoplastic deformation

M.-Carmen Miguel*†, Alessandro Vespignani*, Stefano Zapperi‡, Jérôme Weiss§ & Jean-Robert Grasso‖

** The Abdus Salam International Centre for Theoretical Physics, PO Box 586, 34100 Trieste, Italy*
† Departament de Física Fonamental, Facultat de Física, Universitat de Barcelona, Av. Diagonal 647, 08028 Barcelona, Spain
‡ INFM, Università "La Sapienza", P. le A. Moro 2, 00185 Roma, Italy
§ LGGE-CNRS, 54 rue Moliére, BP 96, 38402 St Martin d'Héres Cedex, France
‖ LGIT, BP 53X, 38041 Grenoble Cedex 9, France

The viscoplastic deformation (creep) of crystalline materials under constant stress involves the motion of a large number of interacting dislocations[1]. Analytical methods and sophisticated 'dislocation dynamics' simulations have proved very effective in the study of dislocation patterning, and have led to macroscopic constitutive laws of plastic deformation[2–9]. Yet, a statistical analysis of the dynamics of an assembly of interacting dislocations has not hitherto been performed. Here we report acoustic emission measurements on stressed ice single crystals, the results of which indicate that dislocations move in a scale-free intermittent fashion. This result is confirmed by numerical simulations of a model of interacting dislocations that successfully reproduces the main features of the experiment. We find that dislocations generate a slowly evolving configuration landscape which coexists with rapid collective rearrangements. These rearrangements involve a comparatively small fraction of the dislocations and lead to an intermittent behaviour of the net plastic response. This basic dynamical picture appears to be a generic feature in the deformation of many other materials[10–12]. Moreover, it should provide a framework for discussing fundamental aspects of plasticity that goes beyond standard mean-field approaches that see plastic deformation as a smooth laminar flow.

Whenever dislocation glide is the dominant plastic deformation mechanism in a crystalline material, we observe a constant strain-rate regime usually described by Orowan's relation $\dot{\gamma} \approx \rho_m b v$. Here, the plastic strain-rate of the material $\dot{\gamma}$ is simply related to average quantities such as ρ_m, the density of mobile dislocations, and v, their